





Optimal fractional-order PID controller of inverter-based power plants for power systems LFO damping

Mahdi SAADATMAND¹, Babak MOZAFARI^{1,*},
Gevork B. GHAREHPETIAN², Soodabeh SOLEYMANI¹

¹Department of Electrical Engineering, Science and Research Branch, Islamic Azad University, Tehran, Iran

²Department of Electrical Engineering, Amirkabir University of Technology, Tehran, Iran

Received: 05.07.2019

Accepted/Published Online: 01.10.2019

Final Version: 27.01.2020

Abstract: The penetration of inverter-based power plants (IBPPs), such as large-scale photovoltaic (PV) power plants (LPPPs), is ever increasing considering the merits of renewable energy power plants (REPPs). Given that IBPPs are added to power systems or replaced by conventional power plants, they should undertake the most common tasks of synchronous generators. The low-frequency oscillation (LFO) damping through the power system stabilizers (PSSs) of synchronous generators is regarded as one of the common tasks in power plants. This paper proposes an optimal fractional-order proportional-integral-derivative (FOPID) controller implemented in the control loop of IBPPs for LFO damping in power systems. For this purpose, the last version of the generic dynamic model for renewable technologies (GDMRT) is used, which was released by the Western Electricity Coordinating Council (WECC) and Electric Power Research Institute (EPRI). In addition, an LPPP is studied as a case study. The FOPID controller is optimally tuned using the particle swarm optimization (PSO) algorithm in order to produce effective LFO damping. Finally, the performance of this controller is simulated and investigated in a two-area test system, showing the better performance of the LPPP for LFO damping by using the proposed optimal FOPID controller compared to the optimal lead-lag controller and optimal PID controller.

Key words: Inverter-based power plant, large-scale PV power plant, low-frequency oscillation, fractional-order proportional-integral-derivative, power oscillation damper

1. Introduction

Power system structures are undergoing important changes due to ever-increasing penetration of inverter-based power plants (IBPPs) [1]. The dynamic characteristics of IBPPs such as wind power plants (WPPs) and large-scale photovoltaic (PV) power plants (LPPPs) are fundamentally different from those of conventional power plants; therefore, the connection of IBPPs to the power system changes the system dynamic performance [2]. Usually IBPPs are geographically far from loads and are connected to the power system by relatively weak transmission lines. Increasing IBPP penetration in power systems with weak transmission lines raises the probability of power system instability, as well as the possibility of low-frequency oscillations (LFOs) [2–4]. There are some mechanisms indicating the indirect effect of the IBPP on LFOs as follows [2]:

*Correspondence: mozafari@srbiau.ac.ir

- Replacing synchronous generators.
- Influencing the synchronizing forces due to effect of the IBPP on the major path of power flows.
- Interaction of the controls of the IBPP with damping torque of large synchronous generators.

The LFO risk can be increased in a power system that has IBPPs due to the above-mentioned issues. On the other hand, given the replacement of IBPPs with conventional power plants, many of the existing capabilities in synchronous generators, such as LFO damping by the power system stabilizer (PSS), should be obtained by them. Therefore, the IBPPs should be able to damp the LFO through an auxiliary controller such as a power oscillation damper (POD). A large body of research has been conducted on LFO damping through LPPPs and WPPs [5–7]. However, no general method has been developed so far for LFO damping in power systems using IBPPs.

In the past decades, different control methods have been suggested. Among them, the proportional-integral-derivative (PID) control method is widely recognized as one of the simplest and most effective ones in industry [8]. The generalization of a conventional PID controller is the fractional-order PID (FOPID) controller. This controller is based on fractional-order calculus, which is an effective tool for modeling many phenomena in engineering [9]. The FOPID controller provides better control performance than the conventional PID controller due to extra degrees of freedom resulting from an integrator of fractional order λ and a differentiator of fractional order δ [9]. Simple structure, more design flexibility, large stability region, better setpoint tracking, high disturbance rejection, and high capability of handling model uncertainties in nonlinear and real-time applications are some advantages of this controller [10]. The FOPID controller has significantly been considered as a new approach in electrical power engineering [10]. In many power systems studies, the FOPID controller has been used as follows:

- Controller for load frequency control [11, 12].
- FOPID-based PSS of synchronous generator [13].
- FOPID-based FACTS damping controller [14, 15].
- Controller for automatic generation control [16].
- Central controller for integrated power system [17].

This study proposes a novel general method for LFO damping by IBPPs, which is based on the design of an optimal FOPID controller implemented in the generic dynamic model for renewable technologies (GDMRT). The FOPID controller parameters are determined using the particle swarm optimization (PSO) algorithm. In order to optimize and determine the controller parameters, an objective function (OF) is defined for a wide range of fault and loading conditions. Given that the GDMRT dynamic model is a strongly nonlinear model, the OF is defined based on the integral of the time-weighted absolute error (ITAE) as a nonlinear function in the time-domain. The rest of this paper is organized as follows. Section 2 describes the IBPP model for stability studies. Section 3 presents the FOPID controller and the concept of the fractional-order calculus. Section 4 explains the implementation of the FOPID controller in an IBPP, as well as its model. The design of an optimal FOPID for an IBPP and the assessment of its performance in a case study are elaborated in Section 5. Finally, the conclusion is provided in Section 6.

2. IBPP models

2.1. IBPP model for power-flow studies

Each IBPP consists of components called renewable energy generators (REGs), which should be modeled for power-flow studies. The REGs within the IBPP such as PV generators (PVGs) or wind turbine generators (WTGs) are modeled in a single generator for power-flow studies, called the “simple aggregated model” [18]. This model has an MVA rating equal to the total MVA rating of individual generators and is connected to the point of common coupling (PCC), as illustrated in Figure 1. Furthermore, since the generators have reactive power generation/absorption capability, the IBPP is considered the same as a synchronous generator for power-flow studies, i.e. its bus is a PV or PQ bus with proper MVA limit [19].

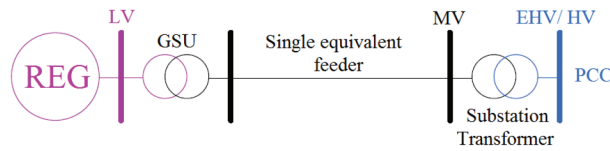


Figure 1. Simple aggregated model of IBPP [18].

2.2. IBPP model for dynamic analysis

A standard, generic, and flexible model must be used for different types of IBPPs in power simulation software [18]. Different models such as the first-generation generic model (FGGM) have been suggested for WPPs [20]. Each of them has been limited to a particular type of IBPP, such as LPPP or WPP, and cannot be used for other types of IBPPs. Based on user experiences with the FGGM for WPP [20], the Western Electricity Coordinating Council (WECC) and Renewable Energy Modeling Task Force (REMTF) released the second-generation generic model (SGGM) for LPPPs and WPPs in 2012 and 2014 [21, 22], which have been used for power system simulation in North America. Regarding the increasing tendency in application of various types of IBPPs, the WECC and Electric Power Research Institute (EPRI) have conducted some studies to present a general dynamic model for IBPPs, called GDMRT [18, 23]. Ultimately, an initial model was developed in 2016 [18]. The GDMRT, which is based on the SGGM, is used for dynamical modeling of different types of IBPPs [18]. Figure 2 demonstrates the modular structure of the GDMRT. As illustrated, this model includes three control modules [18, 23]:

- The renewable energy generator/converter (REGC_A).
- The renewable energy electrical control (REEC_B).
- The renewable energy plant control (REPC_B) or central controller model.

It is worth noting that the GDMRT does not consider any detailed solar irradiation or aerodynamics models. Thus, the solar irradiation or wind speed is assumed to be constant for stability studies during 10–20 s. Additionally, the DC/DC converter is neglected in this model. It should be noted that the inverter of the IBPP is modeled as a current-controlled current source in power system stability analysis.

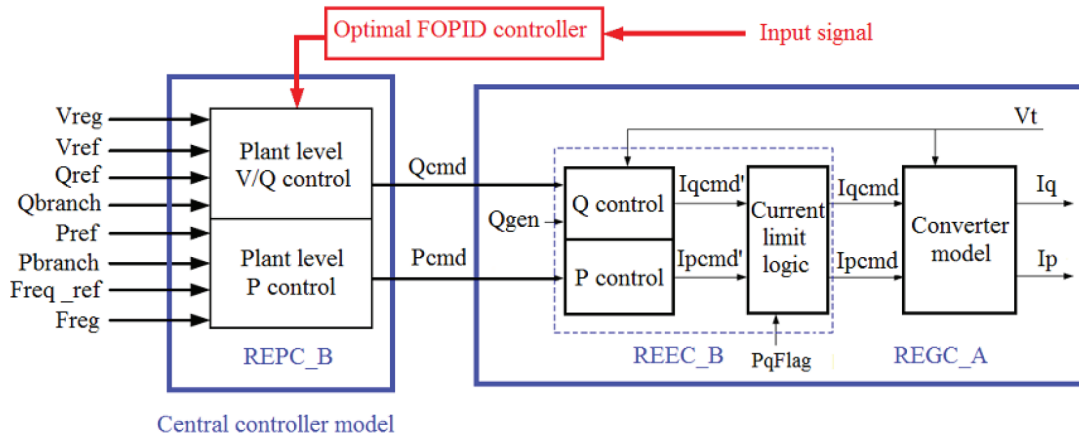


Figure 2. Modular structure of GDMRT [18, 23].

3. FOPID controller

3.1. Fractional-order calculus

Fractional-order calculus is a famous and old mathematical topic that generalizes conventional integer calculus into arbitrary orders. This topic has a history of more than 300 years, yet its applicability in different domains has been realized only recently [10]. Fractional differential equations based on fractional-order calculus have emerged as one of the most important areas of interdisciplinary interest in recent years. The fractional-order differentiator, which can be denoted by a general fundamental operator as a generalization of differential and integral operators, is defined as follows [9, 10]:

$${}_a D_t^q = \begin{cases} \frac{d^q}{dt^q} & , q > 0 \\ 1 & , q = 0 \\ \int_a^t (d\tau)^{-q} & , q < 0, \end{cases} \quad (1)$$

where q represents the fractional order, which can be a complex number, and a and t are the limits of operator D . There are three common definitions for the general fractional differentiation and integration in engineering: the Grunwald–Letnikov (GL) definition, the Riemann–Liouville (RL) definition, and the Caputo definition, in which the GL definition is described as follows: [10, 12]:

$${}_a D_t^q f(t) = \lim_{h \rightarrow 0} \frac{1}{h^q} \sum_{j=0}^{\lfloor \frac{(t-a)}{h} \rfloor} (-1)^j \binom{n}{j} f(t - jh), \quad (2)$$

$$\binom{n}{j} = \frac{\Gamma(n+1)}{\Gamma(j+1)\Gamma(n-j+1)}, \quad (3)$$

where q is between $n-1$ and n (n is the integer value that satisfies the condition), the Γ function indicates the well-known Euler gamma function, and $\lfloor \cdot \rfloor$ represents a floor function.

The RL definition is described as follows [10]:

$${}_a D_t^q f(t) = \frac{1}{\Gamma(n-q)} \frac{d^n}{dt^n} \int_a^t \frac{f(\tau)}{(t-\tau)^{q-n+1}} d\tau, \tag{4}$$

where q is between $n-1$ and n . In addition, there is another definition of the fractional differintegral introduced by Caputo in 1967. The Caputo definition can be written as follows [10]:

$${}_a D_t^q f(t) = \frac{1}{\Gamma(n-q)} \int_a^t \frac{f^n(\tau)}{(t-\tau)^{q-n+1}} d\tau, \tag{5}$$

where q is between $n-1$ and n .

Since it is not easy to use a fractional-order differential equation in a numerical simulation, these equations need to be transformed into the Laplace domain.

3.2. FOPID controller structure

The fractional differential equation of a FOPID controller is described as follows [10, 12]:

$$Y(t) = K_P R(t) + K_I D_t^{-\lambda} R(t) + K_D D_t^\delta R(t). \tag{6}$$

Also, its continuous transfer function in Laplace domain is in the form of [10]:

$$C(S) = \frac{Y(S)}{R(S)} = K_P + K_I S^{-\lambda} + K_D S^\delta, \tag{7}$$

where $C(S)$ is the transfer function of FOPID controller, $R(S)$ is the input signal, and $Y(S)$ is the controller output. Also, K_P , K_I , and K_D represent the proportional, integral, and derivative gains, respectively. Furthermore, λ and δ display the orders of the integral and derivative, respectively. Figure 3a shows the structure of the FOPID controller in a feedback loop [10]. The FOPID controller is an expansion of the PID controller from a point in the λ - δ plane to a square in the same plane. Figure 3b exhibits the graphical representation of the FOPID controller [10]. This expansion provides more flexibility and robustness for the system.

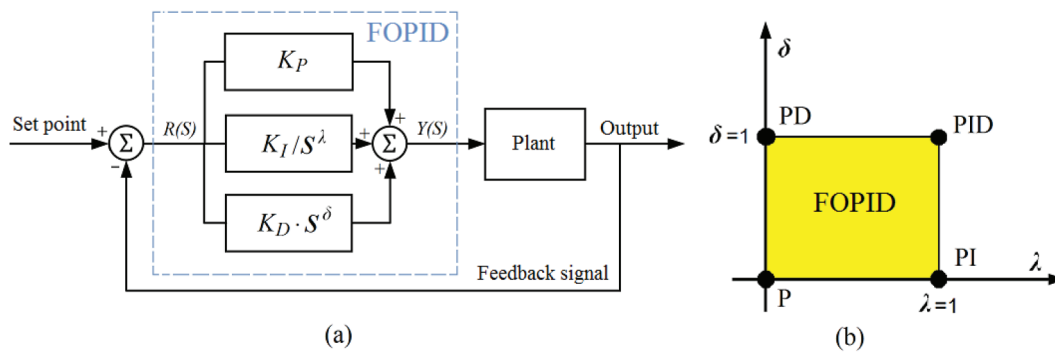


Figure 3. FOPID controller: (a) general structure in a feedback loop; (b) graphical representation in λ - δ plane [9].

4. FOPID controller for LFO damping in IBPP

In this paper, the FOPID controller is proposed as a POD controller for LFO damping in IBPPs. As shown in Figure 4, two different positions are suggested for the FOPID in the central controller model of the GDMRT-based IBPP. Selection of each of these positions is determined based on the operation mode of the IBPP. It should be noted that these positions have been defined as auxiliary inputs in the central controller model for various applications [18, 23].

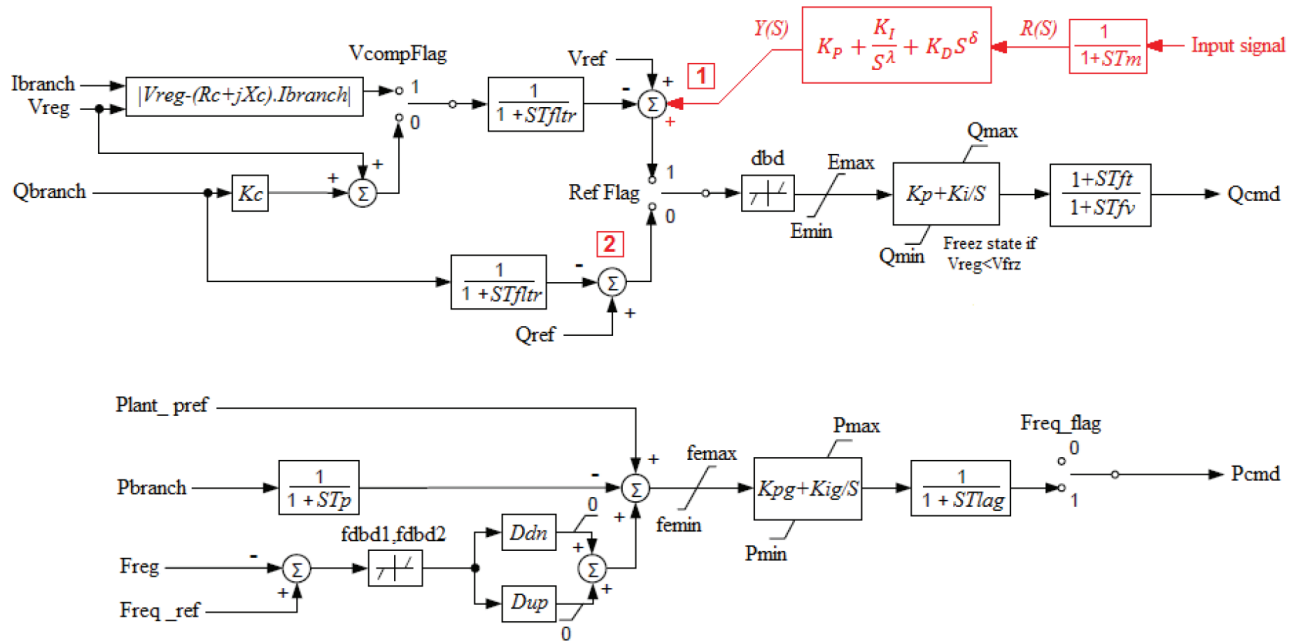


Figure 4. Central controller model of IBPP (REPC_B) based on GDMRT with FOPID controller [18, 23].

Position 1 in Figure 4 is recommended as the FOPID controller placement position if the IBPP operation mode is voltage control mode, or the PCC is considered as a PV bus. Position 2 is proposed as the FOPID controller placement position when the IBPP operation mode is the reactive power control mode or the PCC is used as the PQ bus. In position 1, the signal type injected by the FOPID controller is voltage type, while its type is reactive power in position 2. Furthermore, the stated modes in this section are related to the reactive power/voltage mode control while the active power/frequency control mode is not related to the placement position of the FOPID controller. As mentioned in Section 5.3, implementing a FOPID controller for LFO damping improves the power system response in terms of damping ratio, settling time, overshoots, and undershoots. In addition, this controller is robust to changes of power system parameters.

5. Designing a FOPID controller: a case study using LPPP as IBPP

5.1. Test system

The present study uses a two-area test system as a benchmark system [24]. As indicated in Figure 5, this system includes four synchronous generators modeled by a sixth-order dynamic model and equipped with a simplified IEEE type ST1A excitation system. Furthermore, the conventional type STAB1 PSS is modeled in excitation systems of generators G2 and G4 [25]. Further, the IBPP is connected to bus 6. The rating of the LPPP is

400 MVA. Given that the replacement scenario of the LPPP is considered instead of the conventional power plant, 400 MVA rated power of generator G2 is reduced from 900 MVA to 500 MVA. Then all system loads are considered with a constant power model. Other information related to the two-area test system is given in [25].

It should be noted that many studies have used the two-area benchmark system to evaluate POD performance [5–7]. On the other hand, for proper IBPP performance in LFO damping, the MVA rating of the IBPP should not be negligible compared to the total MVA rating of power system generators [26, 27]. In this study, the MVA rating of the IBPP is equal to 400 MVA/300MW (the capacity of current IBPPs is less than 1000 MW); therefore, the two-area test system can be a good option for evaluating the IBPP performance in LFO damping.

This system is equipped with a wide area measurement system (WAMS) under secure communication technology [28]. The phasor measurement units (PMUs) are used for measuring the necessary signals and placed at the buses of synchronous generators. The measured signals are sent to the FOPID controller via communication channels. Thus, it is necessary to consider the constant time delay. Since the proposed controller is placed at the LPPP, the signal transmission delay between the PMU and FOPID controller should be considered as a constant time delay, where T_m equal to 100 ms is defined for controller design [28]. The input signal of the FOPID controller is considered as the variation of generator speed across the two areas ($\Delta\omega$) [28, 29]. As mentioned, given that the operation mode of the IBPP can be voltage control or reactive power control for power flow, the PCC bus can be modeled as a PV bus or PQ bus, respectively. In this paper, the operation mode of the LPPP is considered in voltage control mode at plant level [21, 23]. In this mode, the PCC is a PV bus and position 1 is considered for FOPID controller placement. Furthermore, the active power control mode is selected as the frequency control at plant level [21, 23].

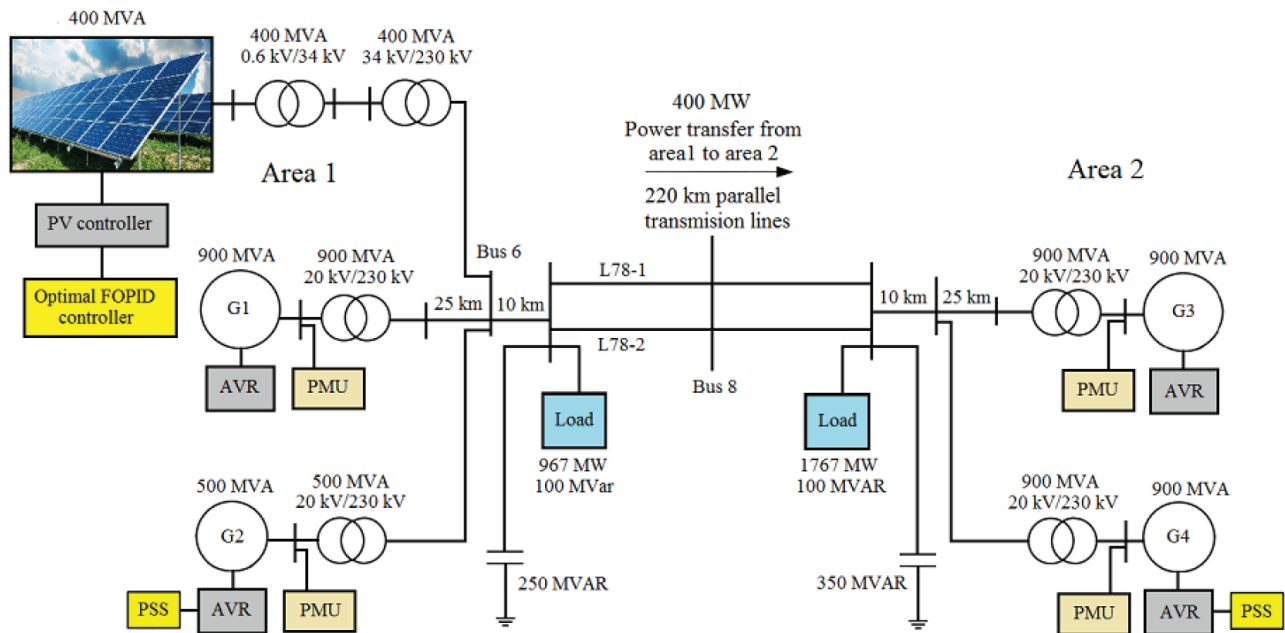


Figure 5. Two-area test system with LPPP as IBPP.

5.2. Designing optimal FOPID controller using PSO

The five parameters K_P , K_I , K_D , λ , and δ should be optimally determined for designing an optimal FOPID controller. Optimal tuning of the FOPID controller is challenging because there are five parameters to tune, which means two more parameters as compared to conventional PID controllers [30]. Different methods have been suggested to optimize the FOPID controllers. One of the most important of these methods is the PSO algorithm. This algorithm is a powerful method for solving optimization problems. PSO is proved to be robust in solving problems featuring nonlinearity, multiple optima, and high dimensionality [30]. Other benefits of the PSO are its relative simplicity and stable convergence characteristic with good computational efficiency [30]. Since the GDMRT is strongly nonlinear and the number of optimization parameters is high [18, 23], the PSO algorithm is used in this study. This optimization algorithm is based on constructing a number of swarm particles and formulating the OF to evaluate the compatibility of each particle in each iteration. The PSO algorithm obtains the optimal values of the parameters of the FOPID controller automatically. Consequently, an optimization problem, which is converted to the OF, should be solved in this regard. The controller should maximize damping and minimize the overshoots, undershoots, and settling times during LFO occurrence. In this paper, the ITAE is used as an index to define the OF, as follows [31–33]:

$$OF = \sum_{F=1}^{N_F} \sum_{L=1}^{N_L} (ITAE)_{FL}, \quad (8)$$

where N_L represents the number of loading conditions and N_F indicates the number of fault conditions. ITAE is defined as follows [33]:

$$ITAE = \int_0^{t_{sim}} t \cdot |e(t)| dt, \quad (9)$$

where t indicates the time variable and t_{sim} shows the simulation time, which is 20 s in this study. Also, $e(t)$ is the error function. Given that there are many generators in the power systems, the OF should be considered as the impact of all generators in optimal FOPID controller design. The sum of the speed deviation of all generators [31] or the sum of the speed difference of the generators [32] can thus be considered as an error function in the ITAE equation. In large power systems, the error function can be defined as follows [31]:

$$|e(t)| = \sum_{G=1}^{N_G} |\Delta\omega_G(t)|, \quad (10)$$

where N_G represents the number of power system generators and $\Delta\omega_G$ represents the speed deviation of generator G . In this paper, the error function is considered as follows [29]:

$$|e(t)| = (|w_1(t) - w_2(t)| + |w_1(t) - w_3(t)| + |w_1(t) - w_4(t)| + |w_3(t) - w_4(t)|). \quad (11)$$

Now we should minimize (8) subject to the controller parameters constraints. The constraints of FOPID controller parameters are as follows:

$$10 < K_P, K_I, K_D < 100, \quad (12)$$

$$0 < \lambda, \delta < 1. \quad (13)$$

The parameters of the FOPID controller are optimized by evaluating the OF and considering multiple fault and loading conditions. In the fault condition, the optimization process is implemented by applying large and small disturbances to the power system as fault conditions 1 and 2, respectively [31]. It should be noted that, in large power systems, various large disturbances can be considered as different fault conditions.

In this study, a temporary three-phase short circuit and a temporary tie-line outage are considered as large and small disturbances, respectively. Tables 1 and 2 present the fault and loading conditions. It should be noted that the loading conditions should be defined based on steady-state stability.

Table 1. Two fault conditions.

Dynamic fault condition no.	Event
1	A temporary 150 ms duration three-phase short circuit at bus 8
2	A temporary 150 ms duration outage of tie-line L78-1

Table 2. Three loading conditions (pu).

Loading condition	L7 and L9
State 1	Nominal loading
State 2	90% of nominal loading
State 3	120% of nominal loading

In order to obtain better efficiency, the number of iterations, number of particles, particle size, c_1 , c_2 , w_{max} , w_{min} , and c are chosen as 100, 20, 5, 2, 2, 0.9, 0.4, and 1, respectively. Different stages of the optimization algorithm are illustrated in Figure 6a. The PSO algorithm is run and then the optimal set of the FOPID controller parameters is selected. The best value of OF is equal to 0.173252. The convergence curve of the OF is shown in Figure 6b. Table 3 lists the optimal values of controller parameters.

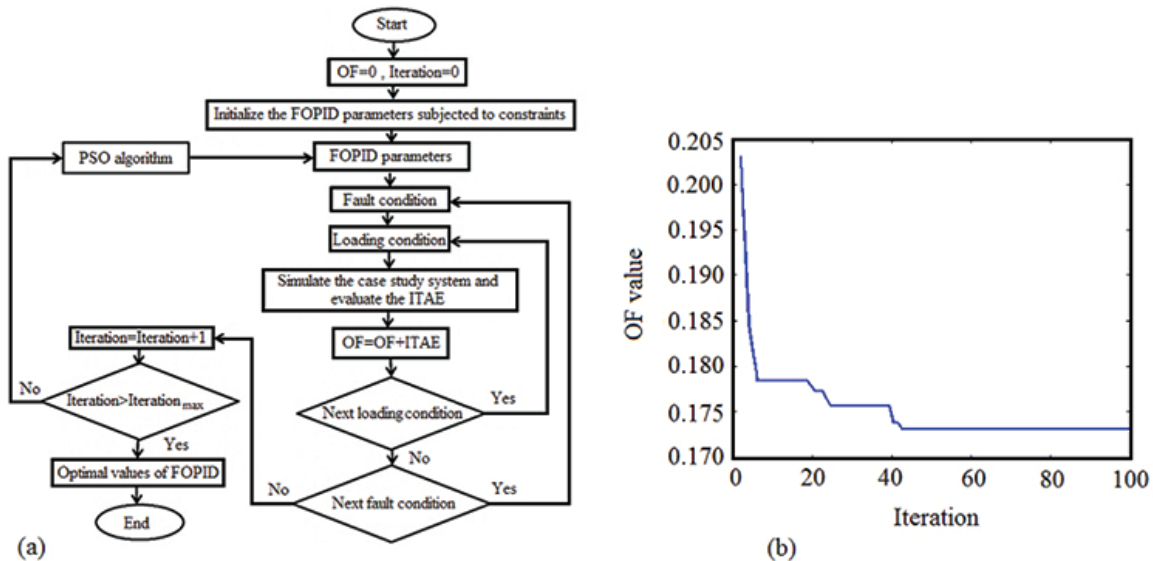


Figure 6. PSO implementation: (a) different stages of the optimization algorithm; (b) convergence curve of OF.

Table 3. Optimal values of FOPID controller parameters.

FOPID controller parameter	Optimal value
K_P	37.784
K_I	23.672
K_D	70.286
δ	0.573
λ	0.395

It should be mentioned that the optimization steps are based on data exchange between MATLAB and DIGSILENT PowerFactory software. The computations were performed by an Intel Core2 Duo CPU (2.00 GHz) with installed memory (RAM) of 2.00 GB. The computation time of optimal parameters was 9960 s.

5.3. Simulation results

This section addresses four cases for assessing the performance of the FOPID controller for LFO damping in the LPPP. The cases are determined in such a way that they can be different in the severity of the disturbance, although they all cause LFO in the power system. These cases are summarized as follows:

- Case I: A 3-phase fault at bus 8 for 170 ms.
- Case II: Outage of tie-line L78-1 at $t = 1$ s for 4 cycles (67 ms).
- Case III: Outage of generator G1 at $t = 1$ s for 4 cycles (67 ms).
- Case IV: Outage of load L9 at $t = 1$ s for 4 cycles (67 ms).

In each case, a disturbance is defined to evaluate the performance of the optimal FOPID controller. In the following, the simulation results are presented for two different modes:

- LPPP with optimal FOPID controller.
- LPPP without optimal FOPID controller.

The simulation results are shown in Figures 7, 8, and 9. Results demonstrate that although the proposed optimal FOPID controller is designed for specific cases, it can also damp out LFO under other disturbances introduced by cases I–IV.

5.3.1. Different loading conditions

Evaluating the performance of the optimal FOPID controller in the different cases at different loading conditions is necessary since they are regarded as one of the factors that may cause changes in operating conditions. For this aim, the numerical index of ITAE is used. A lower value of this index indicates better LFO damping. In order to calculate the value of this index, the loading conditions are implemented as shown in Table 2. The results of the calculations are illustrated in Figure 10. Regarding the comparison of the graphs, the positive effect of the optimal FOPID controller is confirmed for LFO damping.

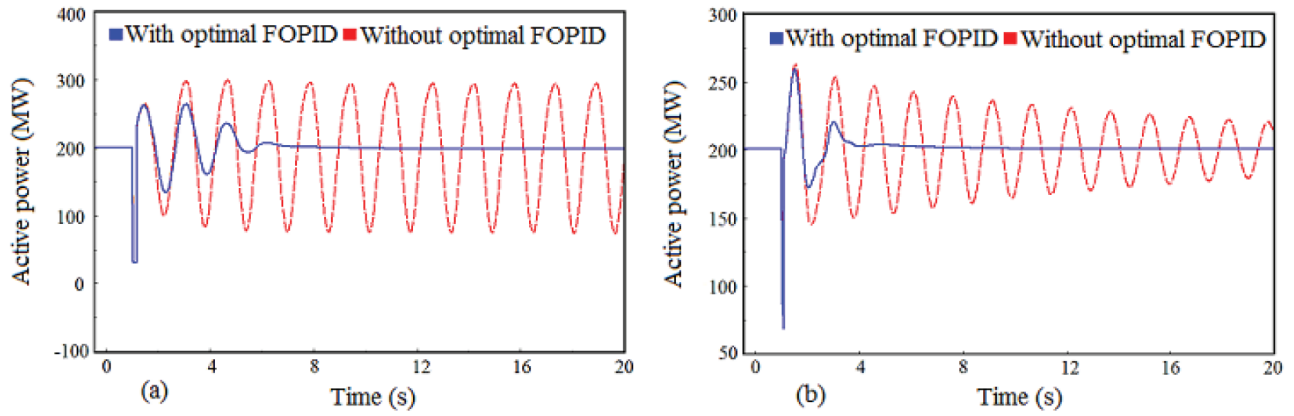


Figure 7. Active power of tie-line L78-2: (a) case I and (b) case III.

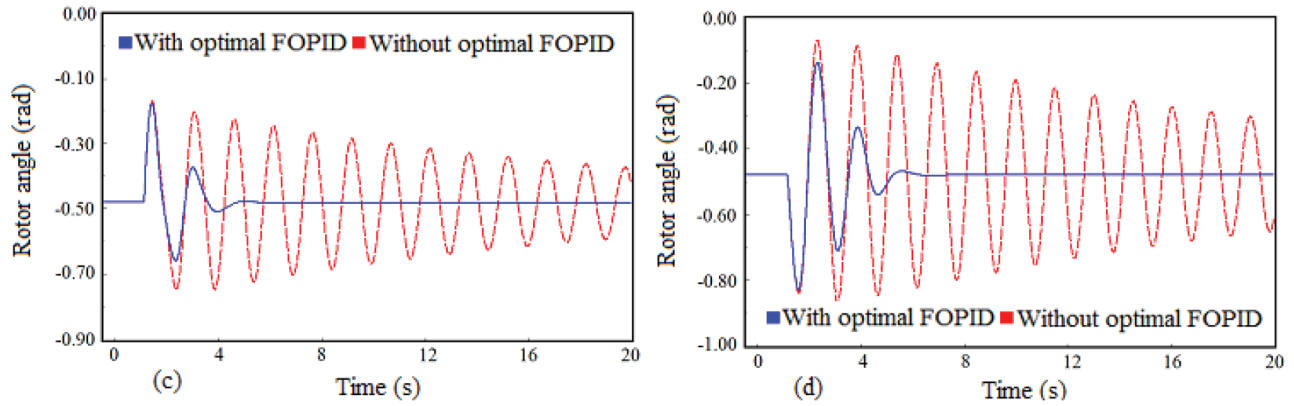


Figure 8. Rotor angle of generator G1: (a) case I, (b) case II, (c) case III, and (d) case IV.

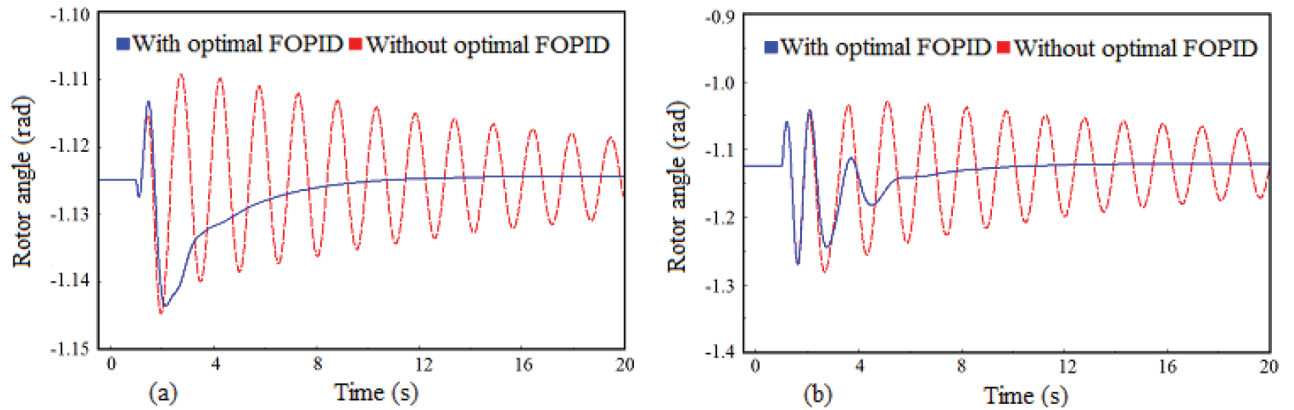


Figure 9. Rotor angle of generator G4: (a) case II and (b) case IV.

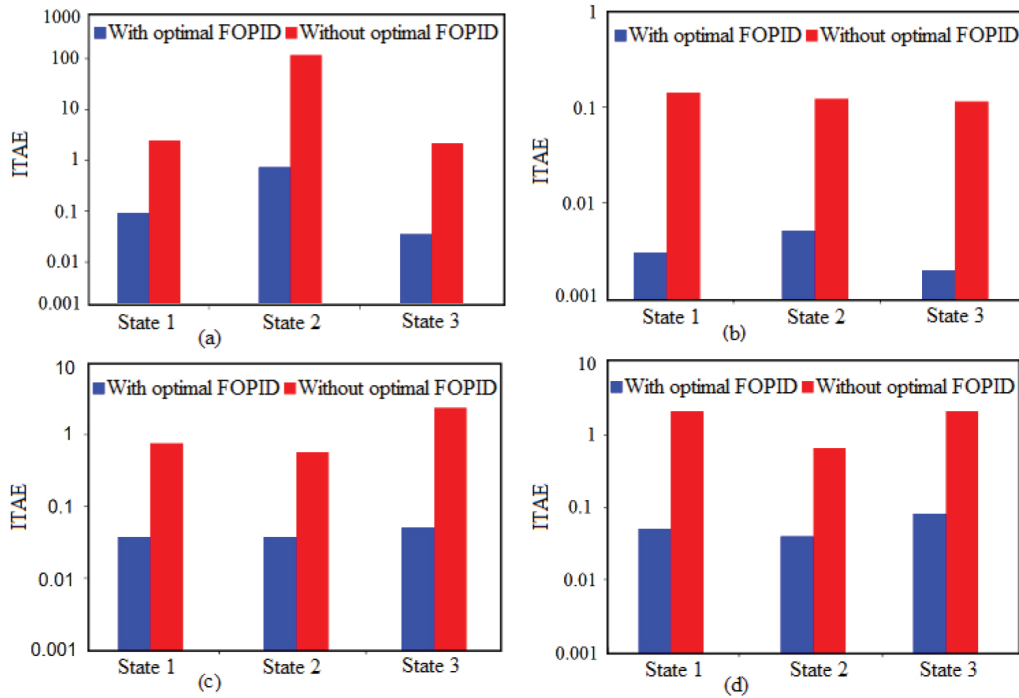


Figure 10. ITAE index: (a) case I, (b) case II, (c) case III, and (d) case IV.

5.3.2. Comparison

One of the common types of PODs is the lead-lag controller, which is used in practical applications. This controller has been proposed in some studies to damp the LFO [6]. Also, the PID controller is a popular controller for electrical applications. Here a comparison is made between the performances of the optimal FOPID controller and these controllers to damp the LFO. In Figures 11 and 12, the comparisons between the performances of these optimal controllers (optimized by PSO algorithm) are shown. It should be noted that the simulation time is considered as 10 s in this subsection. Also, the ITAE index for the optimal FOPID controller, optimal lead-lag controller, and optimal PID controller is obtained in four cases as shown in Figure 13. The results indicate a decrease in the ITAE index value using the optimal FOPID controller.

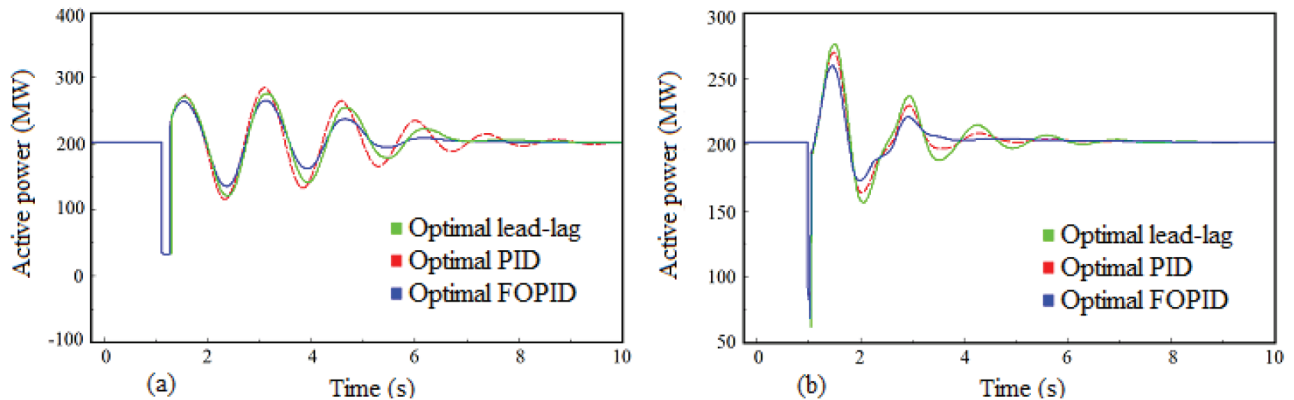


Figure 11. Active power of tie-line L78-2 for different optimal PODs: (a) case I and (b) case III.

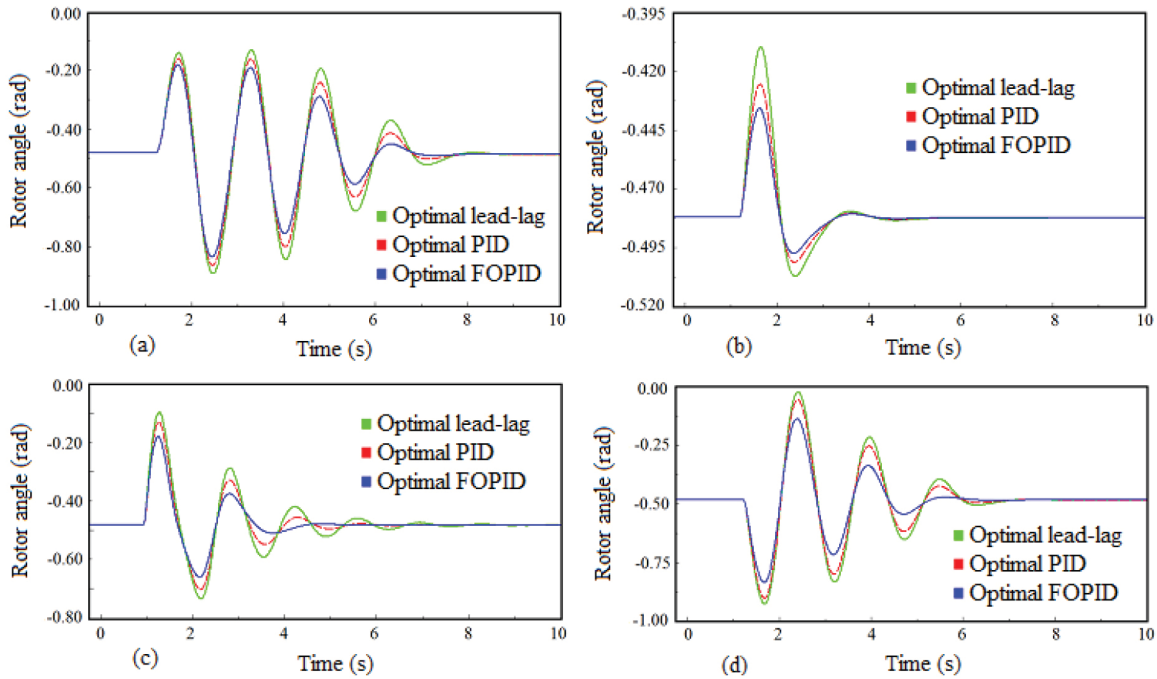


Figure 12. Rotor angle of generator G1 for different optimal PODs: (a) case I, (b) case II, (c) case III, and (d) case IV.

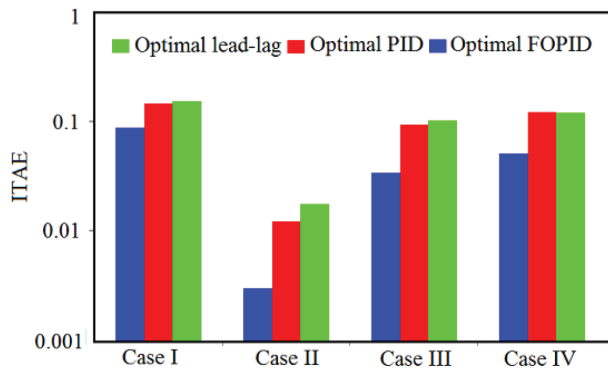


Figure 13. Comparison of optimal PODs in terms of ITAE index in four cases.

Based on the results, connecting the LPPP to the power system decreases the LFO damping and increases its risk sharply. Although it might be possible to restore the LFO damping by resetting the PSSs in the synchronous generators, the power plants should be able to perform LFO damping when REPPs replace synchronous generators over time. Therefore, the proposed optimal FOPID controller is included in this situation and performs the LFO damping. The simulation results show that the application of the optimal FOPID controller for the LPPP improves the damping ratio and settling time in all scenarios. Also, the optimal FOPID controller is more effective in terms of increasing the damping ratio and reducing the overshoot, undershoot, and settling time compared to the optimal PID controller and optimal lead-lag controller.

6. Conclusion

The installation and the development of IBPPs are rapidly increasing with the expanding desire to use REPPs. Given the intrinsic performance of IBPPs and the fact that the structure of these types of power plants is different

from conventional power plants, it is necessary to be able to fulfill many of the inherent tasks of synchronous generators such as LFO damping using auxiliary controllers. The present study has proposed a wide-area measurement-based optimal FOPID controller for IBPPs to effectively damp the LFOs in power systems. The proposed GDMRT-based controller can be implemented on all types of IBPP such as LPPPs and WPPs. In this paper, the LPPP has been considered as an IBPP and the design procedure of the optimal FOPID controller has been presented using the PSO algorithm. The designed optimal FOPID controller has been tested under different conditions in order to verify its performance for LFO damping. Based on the simulation results, the proposed optimal FOPID controller can satisfactorily function under different operating and loading conditions including severe fault conditions. Also, the proposed controller does not have any adverse effect on the power system's transient behavior.

References

- [1] Mueller S, Frankl P, Sadamori K. Next Generation Wind and Solar Power From Cost to Value. Paris, France: International Energy Agency, 2016.
- [2] Quintero J, Vittal V, Heydt GT, Zhang H. The impact of increased penetration of converter control-based generators on power system modes of oscillation. *IEEE Transactions on Power Systems* 2014; 29 (5): 2248-2256.
- [3] Gurung S, Naetiladdanon S, Sangswang A. Probabilistic small-signal stability analysis of power system with solar farm integration. *Turkish Journal of Electrical Engineering & Computer Sciences* 2019; 27 (2): 1276-1289.
- [4] Edrah M, Lo KL, Anaya-Lara O. Impacts of high penetration of DFIG wind turbines on rotor angle stability of power systems. *IEEE Transactions on Sustainable Energy* 2015; 6 (3): 759-766.
- [5] Zhou L, Yu X, Li B, Zheng C, Liu J et al. Damping inter-area oscillations with large-scale pv plant by modified multiple-model adaptive control strategy. *IEEE Transactions on Sustainable Energy* 2017; 8 (4): 1629-1636.
- [6] Singh M, Allen AJ, Muljadi E, Gevorgian V, Zhang Y et al. Interarea oscillation damping controls for wind power plants. *IEEE Transactions on Sustainable Energy* 2015; 6 (3): 967-975.
- [7] Shah R, Mithulananthan N, Lee KY. Large-scale PV plant with a robust controller considering power oscillation damping. *IEEE Transactions on Energy Conversion* 2013; 28 (1): 106-116.
- [8] Sabir MM, Ali T. Optimal PID controller design through swarm intelligence algorithms for sun tracking system. *Applied Mathematics and Computation* 2016; 274: 690-699.
- [9] Podlubny I. Fractional-order systems and $PI^{\lambda}D^{\mu}$ -controllers. *IEEE Transactions on Automatic Control* 1999; 44 (1): 208-214.
- [10] Shah P, Agashe S. Review of fractional PID controller. *Mechatronics* 2016; 38: 29-41.
- [11] Pan I, Das S. Fractional-order load-frequency control of interconnected power systems using chaotic multi-objective optimization. *Applied Soft Computing* 2015; 29: 328-344.
- [12] Taher SA, Fini MH, Aliabadi SF. Fractional order PID controller design for LFC in electric power systems using imperialist competitive algorithm. *Ain Shams Engineering Journal* 2014; 5 (1): 121-135.
- [13] Chaib L, Choucha A, Arif S. Optimal design and tuning of novel fractional order PID power system stabilizer using a new metaheuristic bat algorithm. *Ain Shams Engineering Journal* 2017; 8 (2): 113-125.
- [14] Morsali J, Zare K, Hagh MT. Applying fractional order PID to design TCSC-based damping controller in coordination with automatic generation control of interconnected multi-source power system. *Engineering Science and Technology International Journal* 2017; 20 (1): 1-17.
- [15] Morsali J, Zare K, Hagh MT. A novel dynamic model and control approach for SSSC to contribute effectively in AGC of a deregulated power system. *International Journal of Electrical Power & Energy Systems* 2018; 95: 239-253.

- [16] Pan I, Das S. Fractional order AGC for distributed energy resources using robust optimization. *IEEE Transactions on Smart Grid* 2015; 7 (5): 2175-2186.
- [17] Gupta D, Goyal V, Kumar J. An optimized fractional order PID controller for integrated power system. In: *International Conference on Intelligent Computing and Communication Technologies*; Hyderabad, India; 2019. pp. 663-672.
- [18] Pourbeik P, Sanchez-Gasca JJ, Senthil J, Weber JD, Zadehkhosht PS et al. Generic dynamic models for modeling wind power plants and other renewable technologies in large-scale power system studies. *IEEE Transactions on Energy Conversion* 2017; 32 (3): 1108-1116.
- [19] Delfino F, Procopio R, Rossi M, Ronda G. Integration of large-size photovoltaic systems into the distribution grids: a P-Q chart approach to assess reactive support capability. *IET Renewable Power Generation* 2010; 4 (4): 329-340.
- [20] Ellis A, Kazachkov Y, Muljadi E, Pourbeik P, Sanchez-Gasca JJ. Description and technical specifications for generic WTG models - A status report. In: *2011 IEEE/PES Power Systems Conference and Exposition*; Phoenix, AZ, USA; 2011. pp. 1-8.
- [21] WECC Renewable Energy Modeling Task Force. *WECC Solar PV Dynamic Model Specification*. Salt Lake City, UT, USA: Western Electricity Coordinating Council, 2012.
- [22] WECC Renewable Energy Modeling Task Force. *WECC Second Generation Wind Turbine Models*. Salt Lake City, UT, USA: Western Electricity Coordinating Council, 2014.
- [23] Pourbeik P. *Model User Guide for Generic Renewable Energy System Models*. Palo Alto, CA, USA: Electric Power Research Institute, 2015.
- [24] Canizares C, Fernandes T, Geraldi E, Gerin-Lajoie L, Gibbard M et al. Benchmark models for the analysis and control of small-signal oscillatory dynamics in power systems. *IEEE Transactions on Power Systems* 2016; 2(1): 715-722.
- [25] Kundur P, Balu NJ, Lauby MG. *Power System Stability and Control*. New York, NY, USA: McGraw-Hill, 1994.
- [26] Denholm P, Margolis RM. Evaluating the limits of solar photovoltaics (PV) in traditional electric power systems. *Energy Policy* 2007; 35 (5): 2852-2861.
- [27] Lund PD, Byrne JA, Haas R, Flynn D. *Advances in Energy Systems: The Large-scale Renewable Energy Integration Challenge*. New York, NY, USA: Wiley, 2019.
- [28] Cai D. *Wide area monitoring, protection and control in the future Great Britain power system*. PhD, University of Manchester, Manchester, UK, 2012.
- [29] Kerahroudi SK, Alamuti MM, Li F, Taylor GA, Bradley ME. Application and Requirement of DIgSILENT PowerFactory to MATLAB/Simulink Interface. In: *Gonzalez-Longatt FM, Rueda JL (editors). PowerFactory Applications for Power System Analysis*. Cham, Switzerland: Springer, 2014, pp. 297-322.
- [30] Zamani M, Karimi-Ghartemani M, Sadati N, Parniani M. Design of a fractional order PID controller for an AVR using particle swarm optimization. *Control Engineering Practice* 2009; 17 (12): 1380-1387.
- [31] Das TK, Venayagamoorthy GK, Aliyu UO. Bio-inspired algorithms for the design of multiple optimal power system stabilizers: SPPSO and BFA. *IEEE Transactions on Industry Applications* 2008; 44 (5): 1445-1457.
- [32] Shayeghi H, Safari A, Shayanfar HA. PSS and TCSC damping controller coordinated design using PSO in multi-machine power system. *Energy Conversion and Management* 2010; 51 (12): 2930-2937.
- [33] Nie Y, Zhang Y, Zhao Y, Fang B, Zhang L. Wide-area optimal damping control for power systems based on the ITAE criterion. *International Journal of Electrical Power & Energy Systems* 2019; 106: 192-200.